A Linear Fracture Mechanics Evaluation of Plug Shear Failure

Helena JOHNSSON, Ph.D.
Div. of Timber Structures
Luleå Univ. of Technology
e-mail:
helena.johnsson@ltu.se

M.Sc. in Civil Engineering, 1998. Ph.D. in Timber Structures, 2004, Luleå University of Technology.

Lars STEHN, Ass. Prof.
Div. of Timber Structures
Luleå Univ. of Technology
e-mail: lars.stehn@ltu.se

Ph.D. in Structural Engineering, 1993, Luleå University of Technology. Head of the Div. of Timber Structures at LTU. Lars Stehn has 10 years experience in designing timber structures.

Summary

Brittle failures in mechanical timber joints should be avoided, because this often results in a brittle failure of the structure. Nailed joints experience three ultimate failure modes: embedding, splitting or plug shear failure. Plug shear failure is limiting for nailed connections loaded in tension parallel to the grain. The plug shear failure mode can be divided in two sub-failure modes; tensile and shear failure, where the dominant failure mode is shear.

The aim of the study is to derive a prediction formula for plug shear failure using an engineering linear elastic fracture mechanics approach. Plug shear failure was examined in short-term experiments on nailed steel-to-timber joints in glulam loaded in tension parallel to the grain with varying joint geometries. Test results were compared to theoretical predictions and the results show that the fracture mechanics approach is useful, but needs further development.

Keywords: plug shear failure, nailed timber joints, mixed mode failure in wood

1. Introduction

Timber joints with dowel-type fasteners experience four ultimate failure modes: (a) row shear, (b) plug (block) shear failure, (c) embedding, or (d) splitting, Fig. 1.

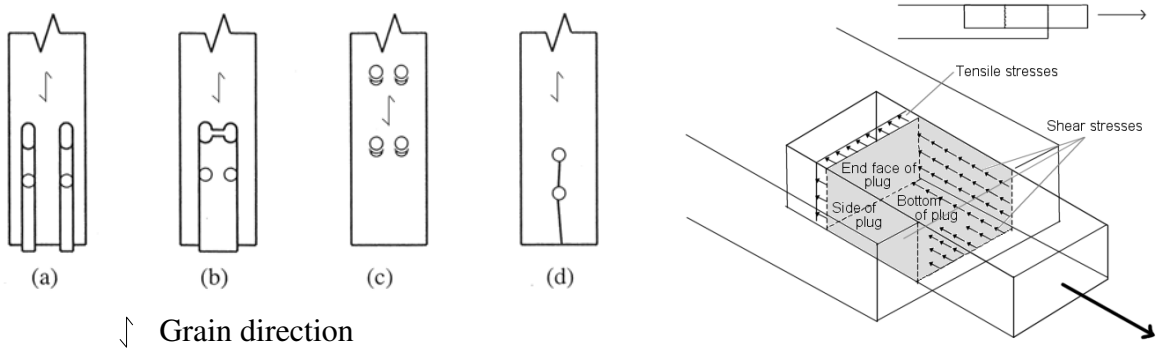

Figure 1 Failure modes in mechanical timber joints, after [1] and schematic plug shear failure.

Embedding failure is a ductile failure mode, while splitting, row shear and plug shear are all brittle failure modes. Splitting has been studied by [2], where a beam on elastic foundation model is used to build a fracture mechanics model describing the behaviour. Row shear and plug shear failure modes were studied by [1]. For nailed joints, embedding and plug shear failure modes dominate for loading in tension parallel to the grain. Earlier prediction models were presented by [3], [4] and [5].

In [5] the course of plug shear failure is described: (1) A crack develops internally along one side of the plug, Fig. 1. The failure is initiated at the nail farthest from the free end, (2) The crack reaches the free end and is visible on the edge. In two-thirds of the experiments this occurs before the ultimate load is reached and (3) The final failure initiates when a shear crack along the bottom face joins the two side cracks.

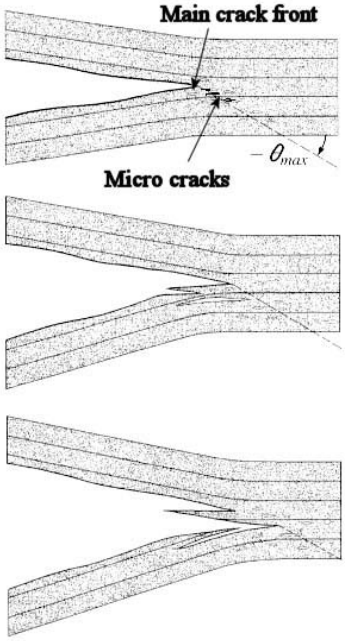

Figure 2 Mixed-mode crack propagation in wood, [6].

In terms of fracture mechanics plug shear failure is a mixed-mode failure, where both opening mode I and shear mode II occur simultaneously. In [6] cracking is described as a process where micro cracks form in front of the main crack front, with the fracture energy being the energy consumed in the process of joining the main crack front and the micro cracks. For pure mode I loading micro cracks form directly in front of the main crack front, while in mixed mode loading, micro cracks form at the maximum principal stress, situated at an angle to the crack plane, Fig. 2. The aim with this paper is to describe plug shear failure as a mixed mode failure within the framework of linear elastic fracture mechanics (LEFM).

2. Materials and Methods

Full size joints in glulam (Picea Abies) were tested in tension parallel to the grain, Fig. 3. The investigation comprised of 5 series, with 5 specimens in each series, totalling 25 specimens. The timber member cross sections were $90 \times 225\text{-}270$ mm^2 ($H \times B$), from European glulam of strength class GL32, [7]. The timber member length varied between 650 and 1100 mm. The specimen consisted of one 10 mm thick steel plate with a yield strength f_y = 355 MPa, annular ringed shank nails with diameter d = 4.0 mm, and nail penetration depth p = 40 mm. Nail holes were pre-drilled with a 3.0 mm-diameter drill.

The GRP- series had nails placed in groups with a distance gd between them. Spacing between nails was 7d parallel to grain and 3.5d perpendicular to grain. The end distance was 80 mm. The specimens were conditioned to a temperature of 20°C and a relative humidity of 65%. Tests were conducted with a time to failure of between 8 and 15 minutes. During testing, load-point displacement δ_{LP}^{II} was measured by two displacement transducers (LVDT, 0 - 50 mm, Vishay) placed centrally in the joint region. Data was sampled with a frequency of 2 Hz. The density and the moisture content were determined on samples taken in the inner lamellas of the joints. The sample size was $40 \times 40 \times 40$ mm^3.

In Table 1, n_c denotes the number of nail columns perpendicular to grain, and n_r is the number of rows parallel to grain. The number of nails (no. of nails) does not equal $n_c \times n_r$ because of the staggered arrangement of the nails, Fig. 3. The effective width, βB, is the width B of the specimen reduced by the edge distances. For the current width B = 270 mm, βB = 126 mm and β = 0.47. The length, L, of the joint includes the end distance 80 mm. In [4], the distance between the two plastic hinges forming in the nail $(\eta H) = (2M_y/(f_h d))^{0.5}$ is taken as a measure of the plug depth. M_y is the plastic moment of the nail and f_h is the embedding strength of timber. For the joints presented in Table 1, ηH = 17 mm i.e. η = 0.19.

Table 1 Specimen characteristics

Series	n_c	n_r	No. of nails	L [mm]	gd [mm]
RECTL	15	19	143	276	-
RECTX0	29	19	276	452	-
GRPS	15	19	143	337	75
GRPL	15	19	143	412	150
GRPX	15	19	143	482	300

3. Results

The failure loads from all 8 test series are presented in Table 2 together with results from the determination of density and moisture content. In Table 2, P_f is the ultimate failure load, δ_{LPf}^{II} is the corresponding displacement, ρ denotes the density, and w the moisture content.

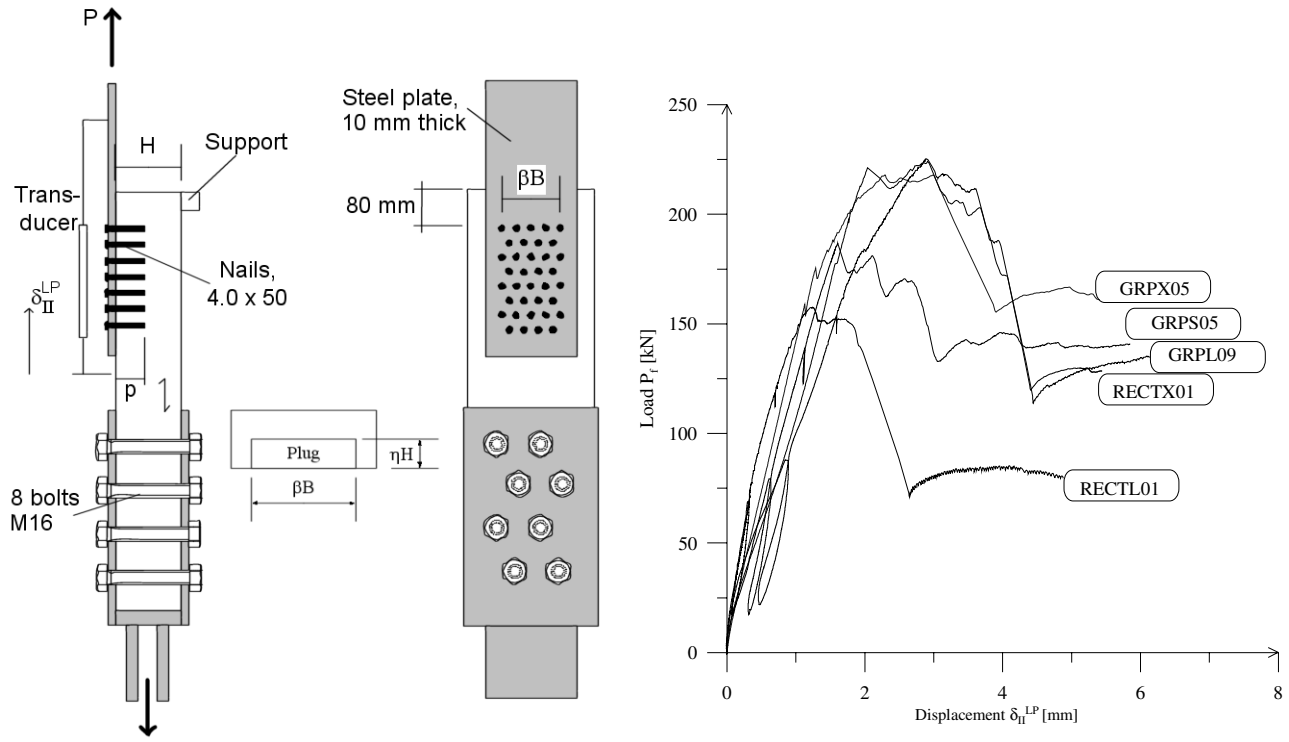

Figure 3 (a) Experimental set-up (b) Experimental load-displacement curves

In Fig. 3b, typical load-displacement curves from the experiments are plotted. Their shapes indicate that plug shear failure is not precisely a brittle failure, but that some reserve capacity exists after the onset of cracking. It is possible that mechanisms for crack arrest are active and that the joint gradually fails after crack propagation starts. The depth of the plug varies between 20-30 mm at the last nail column to 40-60 mm at the free edge of timber. The depth of the plug increases during crack propagation, which is explained by the mixed mode crack propagation presented in [6].

Table 2 Test results

Series	**Failure load, P_f [kN]**	**Displacement, δ_{LPf}^{II} [mm]**	**Density, ρ [kg/m^3]**	**Moisture content, w [%]**
RECTL	150, 158, 162, 167, 171	1.2, 1.2, 1.8, 1.7, 1.3	467, 450, 415, 488, 431	11.1, 10.7, 10.5, 10.7, 11.3
RECTX0	224, 233, 252, 262, 281	2.9, 2.2, 1.8, 2.3, 2.4	441, 431, 456, 420, 455	10.0, 9.30, 10.0, 9.44, 10.1
GRPS	160, 178, 186, 187, 195	1.9, 2.2, 2.7, 1.6, 1.0	475, 472, 434, 458, 455	11.3, 11.2, 10.8, 11.1, 11.4
GRPL	202, 209, 221, 225, 230	2.0, 2.5, 2.6, 2.9, 2.1	422, 485, 446, 480, 465	10.7, 11.9, 11.7, 11.6, 11.4
GRPX	205, 218, 229, 243, 250	4.5, 2.3, 4.0, 2.7, 4.0	409, -, 365, 426, 443	9.19, -, 8.6, 9.33, 9.98

4. Analysis

The linear elastic fracture mechanics (LEFM) approach is valid provided that the crack tip is sharp and the specimen size is sufficiently large compared to the fracture process zone. For mode I failure the fracture zone in wood is typically a few mm, [8], but for mode II failure the fracture zone can amount to several centimetres in length, [8]. At the onset of cracking the LEFM restrictions hold, but during the entire crack propagation the fracture process zone may not be sufficiently small. The developed LEFM model uses the energy formulation of linear elastic fracture mechanics. Under quasi-static conditions and for a single load, Eqn. (1) expresses the failure load:

$$P_f = \sqrt{\frac{2bG_c}{dC/da}} \qquad (1)$$

P_f is the critical or failure load, b the width of the crack, and G_c the critical energy release rate. The linear elastic compliance $C(a) = \delta_{LP}/P$, where δ_{LP} is the load-point displacement due to load P and a is the crack length. For European softwood, G_{Ic} is described as $G_{Ic} = -146 + 1.04\rho$ Nm/m^2, where ρ is the density in kg/m^3, [9]. Test results for the shear failure mode II are more scarce, but $G_{IIc} = 932$ Nm/m^2 is reported by [10] also from tests on European softwood.

For the mixed mode plug shear failure, where both modes I and II occur simultaneously, a failure criterion is necessary. Eqn. 2a was suggested by [11], which is reformulated via the relation $G = K^2/E$ and Eqn. 1 in terms of load as in Eqn. 2b. E is the elastic modulus, K_I and K_{II} are the stress intensity factors and K_{Ic} and K_{IIc} are the corresponding fracture toughnesses. In Eqn. 2b, P_I indicates the mode I opening load acting in the direction perpendicular to grain and P_{II} is the mode II shear load. The critical loads can be established through Eqn. 3 and are denoted P_{Ic} and P_{IIc}.

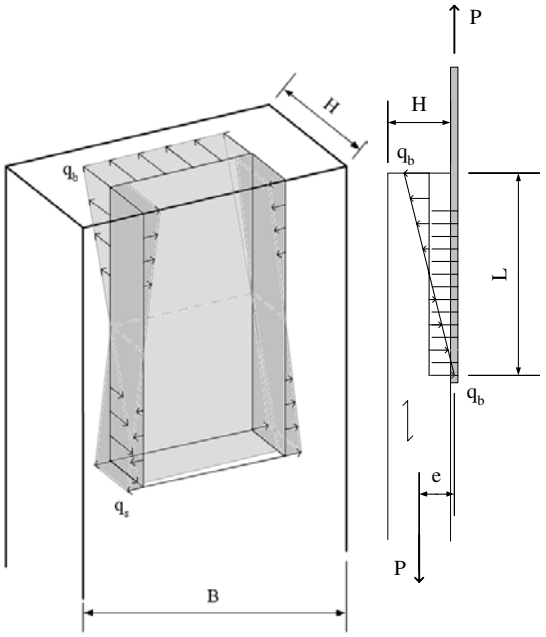

(a) (b)

Figure 5 Load situation in plug a) 3D view b) Moment acting on the side surfaces (e = 50 mm)

$$\frac{K_I}{K_{Ic}} + \left(\frac{K_{II}}{K_{IIc}}\right)^2 \le 1;\ \frac{P_I}{P_{Ic}} + \left(\frac{P_{II}}{P_{IIc}}\right)^2 \le 1 \qquad (2ab)$$

4.1 Load situation in joint

The eccentric moments introduced in the joint by the placement of the nail group are schematically shown in Fig. 5a. Two different flexural loads can be distinguished, q_s and q_b, which act on different surfaces and do not interact. The experimental observations indicate that the side surfaces are not active in the load uptake when the failure load is reached; therefore the analysis focuses on the resistance of the bottom face. The load acting on the bottom face, P_I, is the resultant to the distributed load q_b that can be determined through an equilibrium equation in Fig. 5b shown in Eqn. 3. The load P_{II} is assumed to be P.

$$P_I = \frac{q_b L}{4} = \frac{6Pe}{L^2} \cdot \frac{L}{4} = \frac{3Pe}{2L} \qquad (3)$$

4.2 Derivation of critical failure load

For mode II failure, [12] made one of the first approaches for glued timber lap joints, Fig. 6, Eqn. 4. In Eqn. 4 $\gamma = E_1 t_1/(E_2 t_2) \le 1.0$, where t is the thickness. For the current application, $E_1 = E_2 = E$.

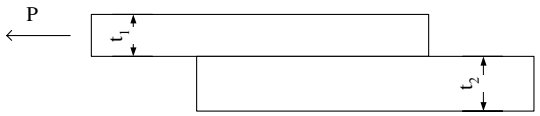

$$P_{IIc} = b\sqrt{2(1+\gamma)}\sqrt{t_1 E_1 G_{IIc}} \qquad (4)$$

Figure 6 Lap joint

To obtain the critical load for mode I loading, the wooden part of the joint is modelled as a beam with cross-sectional area $A = \eta H \times \beta B$, Fig. 7. The model is based on the initial crack approach. The length of the initial crack a, is taken as the diameter of the nail, i.e. $a = 4$ mm. This assumption is nor obvious, since the nail hole is not continuous along the width of the crack. However, it can be shown that the initial crack is created during loading, [13]. The crack is assumed to start at $a = 0$ and propagates towards the free end, $a = L$, Fig. 7. The beam modelling the plug is stubby and therefore both shear and flexural deformations are considered according to Timoshenko beam theory. An expression for deflection δ at the free end of a beam of length a is established and divided by P from Eqn. 3 to obtain the compliance C, which finally is inserted in Eqn. 1 to give the critical load P_{Ic} in Eqn. 5.

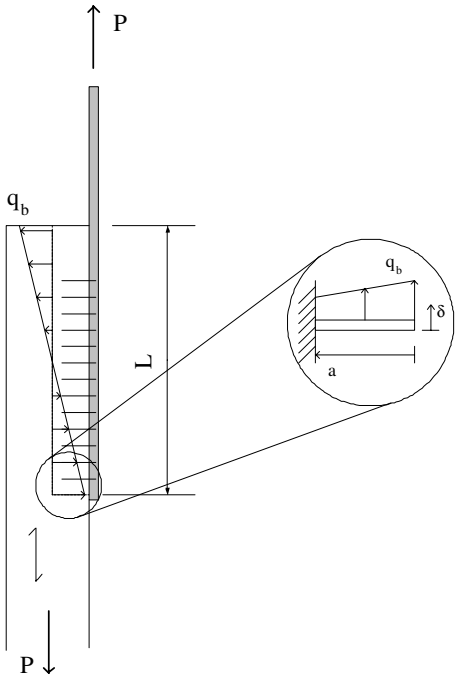

$$P_{Ic} = \beta B \sqrt{\frac{G_I L^2}{\frac{4a^3}{E(\eta H)^3}(3L - 2a) + \frac{2k_T a}{G \cdot \eta H}(L - 2a)}} \tag{5}$$

For rectangular cross sections, the factor $k_T = 5/6$. G is the shear modulus and A the cross sectional area. $I = \beta B \times (\eta H)^3/12$ and $A = \eta H \times \beta B$ was assumed in Eqn. 5.

By inserting the critical loads P_{Ic}, Eqn. 5, and P_{IIc}, Eqn. 4, together with P_I, Eqn. 3, and $P_{II} = P$ into the failure criterion in Eqn. 2b and solving the quadratic equation, a prediction of the failure load, P_f, is obtained. Assuming that $L >> a$, the expression for P_f is given in Eqn. 6. In Fig. 8 the model is compared to experimental results.

$$P_f = -\frac{3e}{4L} \cdot \frac{P_{IIc}^2}{P_I} + \sqrt{\left(-\frac{3e}{4L} \cdot \frac{P_{IIc}^2}{P_I}\right)^2 + P_{IIc}^2}$$
$$\frac{P_{IIc}^2}{P_I} = 2(1+\gamma)\sqrt{\frac{G_{II}^2 E}{G_I G}}\sqrt{\frac{12Ga^3 + 2Ek_T(\eta H)^2 a}{L \cdot \eta H}} \tag{6}$$

Figure 6 Beam model of plug part

5. Discussion

The prediction model in Eqn. 9 is compared to the experimental results in Fig. 8. The model clearly underestimates the plug shear resistance. However, the theoretical model shows the same asymptotic behaviour as the experimental results. The deviation is most probably caused by the softening behaviour of the joints. In LEFM theory a perfectly brittle material behaviour is assumed, but the experiments show reserve capacity after the failure load is reached, Fig. 4b. This means that the fracture energy is higher than in the LEFM case. The softening behaviour of the joint can be considered through the use of either a finite element compliance calibration or a theoretical approach as in [14]. If a theoretical approach is chosen, it might be possible to derive a relation suitable for code format, which is closer to the test results than the failure load curve in Fig. 8.

If the softening behaviour of the joint is taken into account, the curve for the failure load P_f in Fig. 8 will show higher load values. In [13] the influence of the softening behaviour of the joint was studied through an FE compliance calibration. The results showed that the predicted failure load P_f is higher than the LEFM result presented here in. The agreement with experimental results was good, however somewhat risky. The main parameter affecting the calibration results is the stiffness of wood in shear. To the authors knowledge, the effect on shear stiffness caused by joint size has not been studied. This topic is an interesting area for further development of the fracture mechanics modelling of brittle failures in timber joints.

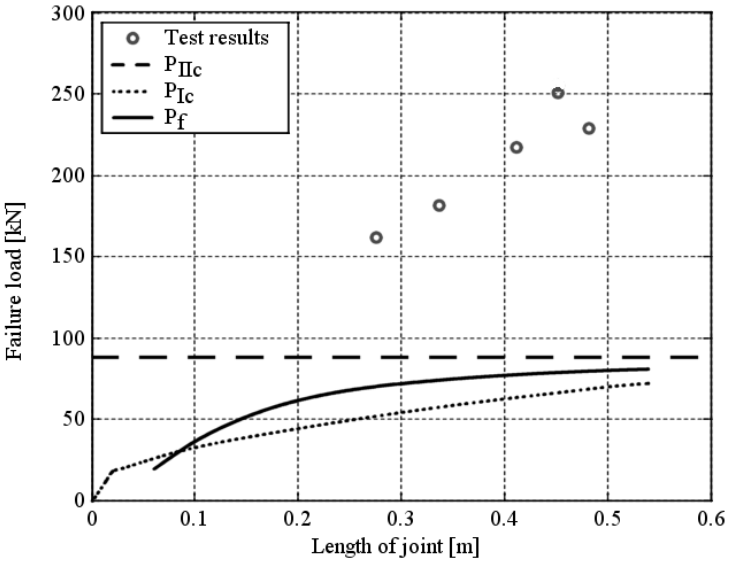

Figure 8 Comparison between theory and experiments

6. References

[1] Quenneville, J.H.P. and M. Mohammad. On the Failure Modes and Strength of Steel-Wood-Steel Bolted Timber Connections Loaded Parallel to Grain. *Canadian Journal of Civil Engineering*.Vol. 27, No.4, 2000, 761-773.

[2] Schmid, M., H.-J. Blass, and R.P.M. Frasson. Effect of Distances, Spacing and Number of Dowels in a Row on the Load Carrying Capacity of Connections with Dowels Failing in Splitting. In: *International Council for Research and Innovation in Building and Construction, Working Commission CIB-W18*, 2002, paper 35-7-5, Kyoto, Japan, September 2002.

[3] Foschi, R.O. and J. Longworth. Analysis and Design of Griplam Nailed Connections. *Journal of the Structural Division*.Vol. 101, No.12, 1975, 2537-2555.

[4] Kangas, J., K. Aalto, and A. Kevarinmäki. Modelling of the Block Tearing Failure in Nailed Steel-to-Timber Joints. In: *International Council for Research and Innovation in Building and Construction, Working Commission CIB-W18*, 1997, paper 30-7-2, Vancouver, British Columbia, Canada

[5] Johnsson, H. Plug Shear Failure in Nailed Timber Connections: Experimental Studies. In: *International Council for Research and Innovation in Building and Construction, Working Commission CIB-W18*, 2003, 36-7-2, Estes Park, Colorado, USA

[6] Jernkvist, L.O. Fracture of Wood under Mixed Mode Loading: Part I. Derivation of fracture criteria. *Engineering Fracture Mechanics*.Vol. 68, No.5, 2001, 549-563.

[7] Eurocode 5 (1998). Eurocode 5 - Design of Timber Structures. ENV 1995-1-1:1993.

[8] Gustafsson, P.-J. Fracture Perpendicular to Grain - Structural Applications. In: S. Thelandersson and H.J. Larsen, Eds. *Timber Engineering*. Wiley & Sons, 2003, ISBN 0-470-84469-8.

[9] Larsen, H.J. and P.-J. Gustafsson. The Fracture Energy of Wood in Tension Perpendicular to the Grain: Results from a Joint Testing Project. In: *International Council for Research and Innovation in Building and Construction, Working Commission CIB-W18*, 1990, paper 23-19-2, Lisbon, Portugal

[10] Riberholt, H., et al. *Timber Beams Notched at the Support*. TVSM-7071, Div. of Structural Mechanics, Lund Institute of Technology, Lund, 1992.

[11] Wu, E.M. Application of Fracture Mechanics to Anisotropic Plates. *Journal of Applied Mechanics*.Vol. 34 E, No.4, 1967, 967-974.

[12] Volkersen, O. Die Nietkraftverteilung in zugbeanspruchten Nietverbindungen mit konstanten Laschenquerschnitten. *Luftfahrtvorschung*.Vol. 15, 1938, 41-47.

[13] Johnsson, H. and L. Stehn. Plug Shear Failure in Nailed Timber Connections: Linear Elastic Fracture Mechanics Modelling. *Submitted to Engineering Fracture Mechanics*, 2004.

[14] Ottosen, N.S. and K.-G. Olsson. Hardening/Softening Plastic Analysis of Adhesive Joints. *Journal of Engineering Mechanics*.Vol. 114, No.1, 1988, 97-116.